Reaction of Hydrogen with Ag(111): Binding States, Minimum Energy Paths, and Kinetics

Alejandro Montoya,* Anna Schlunke, and Brian S. Haynes

School of Chemical and Biomolecular Engineering, The University of Sydney, Sydney, NSW 2006, Australia

Received: May 4, 2006; In Final Form: June 22, 2006

The interaction of atomic and molecular hydrogen with the Ag(111) surface is studied using periodic density functional total-energy calculations. This paper focuses on the site preference for adsorption, ordered structures, and energy barriers for H diffusion and H recombination. Chemisorbed H atoms are unstable with respect to the H_2 molecule in all adsorption sites below monolayer coverage. The three-hollow sites are energetically the most favorable for H chemisorption. The binding energy of H to the surface decreases slightly up to one monolayer, suggesting a small repulsive H−H interaction on nonadjacent sites. Subsurface and vacancy sites are energetically less favorable for H adsorption than on-top sites. Recombination of chemisorbed H atoms leads to the formation of gas-phase H_2 with no molecular chemisorbed state. Recombination is an exothermic process and occurs on the bridge site with a pronounced energy barrier. This energy barrier is significantly higher than that inferred from experimental temperature-programmed desorption (TPD) studies. However, there is significant permeability of H atoms through the recombination energy barrier at low temperatures, thus increasing the rate constant for H_2 desorption due to quantum tunneling effects, and improving the agreement between experiment and theory.

Introduction

Detailed information about H binding states, structural properties, and minimum energy paths for H diffusion and recombination on silver surfaces is important for the chemical understanding and accurate modeling of catalyzed reactions carried out on silver, such as the partial oxidation of hydrocarbons and alcohols, electrochemical processes, and the water gas shift reaction. The hydrogen interaction with metal surfaces has become a model system for experimental and modeling studies of surface reactions.[1−4] This paper contributes to the understanding of the thermodynamics and kinetics of the H_2/Ag(111) for which some uncertainties still remain in the literature and discussed below.

The reaction of hydrogen with silver presents particular chemical and kinetic properties. The dissociative chemisorption of H_2 is highly activated and does not occur on clean Ag(111) at room temperature[5−7] nor on Ag(110)[8] surfaces at a substrate temperatures below 150 K. The dissociation of D_2 on Ag(111) has been reported only using molecular beam scattering at translational energies above 220 meV and gas temperatures above 940 K,[9,10] suggesting a very small sticking coefficient of H_2 to Ag(111) at low kinetic energies consistent with quantum dynamic studies of H_2 on Ag(100).[11]

Recombinative desorption of atoms on Ag(111) occurs at significantly lower temperatures than is seen for other metals, around 200 K, depending on the surface coverage and heating rate. Temperature programmed desorption (TPD) of H_2/D_2 from Ag(111) shows that recombination of H or D atoms does not fit a simple kinetic description. The TPD peak is symmetrical but shifts toward higher temperatures with increasing surface coverage. Zhou et al.,[12] using the leading edge analysis, deduced a half order reaction with a D_2 desorption energy barrier of 6.4 kcal mol^{-1}. Parker et al.[13] used the entire TPD spectrum reported by Zhou et al.[12] and deduced a second-order reaction with a desorption barrier of 10.5 kcal mol^{-1}. Lee et al.[14] used the leading edge analysis of their data to obtain a D_2 desorption energy barrier of 8.7 ± 1.0 kcal mol^{-1}, independent of kinetic order. Healey et al.[15] deduced a D_2 desorption energy barrier of 6.4 ± 0.1 kcal mol^{-1} using the Taylor and Weinberg technique and were able to reproduce their TPD spectrum by assuming a half order reaction.

The reported activation energies from experimental studies of dissociation and recombination kinetics suggest that the dissociative chemisorption of H_2/D_2 to the Ag(111) surface is an endothermic activated process, further implying a rather low Ag−H binding energy. Experimental values for the heat of reaction of H_2 on silver are scarce, but predictions of the Ag−H bond strength and of the heat of reaction have been carried out using quantum chemistry calculations. The DFT-calculated binding energy of Ag−H on cluster structures of the Ag(111) surface shows a considerable fluctuation with the number of Ag atoms, 32.7−46.4 kcal mol^{-1} for 10−25 Ag atom cluster structures[16] and 73.1−92.7 kcal mol^{-1} (23.75−31.5 kcal mol^{-1} after corrections due to the localized electrons) using 4−12 Ag atom cluster structures.[17] Because the experimental binding energy per H atom in the H_2 molecule is 51.63 kcal mol^{-1},[18] the predicted heat of reaction for the H_2 dissociation switches from endothermic to exothermic depending on the Ag−H binding energy selected. Periodic DFT-GGA calculations on Ag(111) yield an Ag−H binding energy of 48.0 kcal mol^{-1} at 1/4 monolayer,[19,20] showing an endothermic process for H_2 dissociation on Ag(111). By comparison, DFT-GGA studies of H_2 dissociation on the Ag(110)[21,22] suggest an endothermic heat of reaction, which is consistent with an Ag−H binding energy of 42.7 kcal mol^{-1} on the Ag(110) facet calculated using an embedded cluster method at the interaction configuration level.[23]

Molecular analysis of the coverage-dependent H binding energy to the Ag(111) surface is limited and the sensitivity of the kinetics of desorption/recombination to surface concentration

* To whom correspondence should be addressed. E-mail: a.montoya@usyd.edu.au.

10.1021/jp062725g CCC: $33.50
Published on Web 08/04/2006

appear not to have been studied. Low-energy electron diffraction (LEED) measurements have shown that chemisorbed H atoms at 100 K form a (2×2) (at 0.25−0.5 ML) and a mixture of (2×2) and (3×3) (at 0.5−0.6 ML) superstructures,[15,24] suggesting similar binding energies at these surface coverages. The surface became saturated with H atoms below full monolayer, showing a highly activated diffusion of H to the bulk of the Ag(111).

This paper provides a comprehensive survey of H on Ag(111). We address the surface occupation, on top and in the subsurface, the site preference for adsorption, ordered structures, and minimum energy paths for the interaction of hydrogen with the Ag(111) surface. We report the quantum tunneling effect on H recombination and its effect on the kinetics of H_2 desorption at low and high temperatures.

Theoretical Calculations

The molecular modeling simulations were performed using the plane-wave density functional theory (DFT) code Dacapo[25,26] with Vanderbilt ultrasoft pseudo-potentials.[27] The Perdew and Wang nonlocal corrections to the exchange-correlation energy were included self-consistently.[28] The Kohn−Sham equations[29] were solved using a plane-wave basis set of kinetic energy 340 eV, while 400 eV was used as a cutoff for the density grid. In test calculations, for higher kinetic-energy values, a density cutoff equal to the kinetic energy was used. A Monkhorst−Pack mesh[30] of $(6 \times 6 \times 1)$ k points was used for the (2×2) unit cell. The k point density was maintained as constant as possible for calculations using various unit cell sizes to allow quantitative comparison of surface energetics. Test calculations were performed to check the convergence of the binding energy of the hydrogen atom on top of the Ag(111) surface at 0.5 coverage. The kinetic energy cutoff was increased up to 680 eV, and the k point was increased up to $(8 \times 8 \times 1)$. The resulting change in the binding energy was less than 0.3 kcal mol^{-1}.

The Ag surface is represented by periodic slabs with five layers repeated in a supercell geometry with 15 Å of vacuum between them. The three lower layers are maintained at DFT-bulk geometry (the DFT calculated Ag lattice constant is 4.14 Å vs 4.09 Å experimentally[18]), and the two upper Ag atom layers are allowed to relax fully. The adsorbate is chemisorbed and fully relaxed on the upper layer of the Ag slab and the induced dipole moment is taken into account by applying a dipole correction.[31] Four different unit cells have been used, (1×1), (2×2), $(\sqrt{3} \times \sqrt{3})$R30, and (3×3), to represent surface coverages of 1.0, 0.25, 0.33, and 0.11 monolayer, respectively, using one hydrogen atom per unit cell. The (2×2) unit cell is also used to represent surface coverages of 0.5 and 0.75 using two and three hydrogen atoms, respectively. The optimization is achieved when the root-mean-square force on the atomic nuclei was less than 0.05 eV/Å. The self-consistent field was carried out using an electronic temperature of $k_BT = 0.1$ eV and $k_BT = 0.0001$ eV for the Fermi distribution of the slabs and gas-phase molecules, respectively, with Pulay mixing of the resulting electronic density. Total energies have been extrapolated to $k_BT = 0$ eV. The total energies of isolated H and H_2 are calculated in a cubic cell of side length 12 Å. When spin polarization corrections are included, the absolute energies of H and H_2 are −13.9067 and −31.7926 eV, respectively. For the hydrogen molecule, a bond length of $r(H-H) = 0.7533$ Å and a frequency value of $\upsilon = 4450$ cm^{-1} are calculated. The binding energy for H in H_2 is calculated to be $E_{B-DFT} = 49.55$ kcal mol^{-1} including the H_2 zero point energy (ZPE), and 52.73 excluding the H_2 ZPE. Experimental values are $r(H-H) = 0.7417$ Å, $\upsilon = 4405$ cm^{-1}, and $E_B - \exp = 51.63$ kcal mol^{-1}.[18]

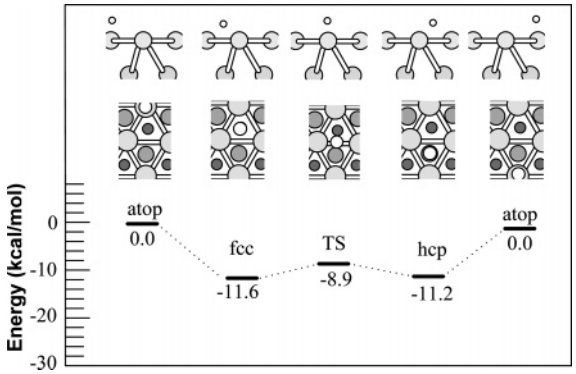

Figure 1. Minimum Energy Path (MEP) at 0 K of H diffusion on symmetric sites of the Ag(111) surface. The inset figure shows the H positions on a subset of the Ag(111) surface. Hydrogen atoms are represented as small white circles on atop, fcc, bridge (TS), and hcp sites.

The minimum energy paths (MEP) on the potential energy surface for the different reaction channels are calculated using the nudged elastic band (NEB) method.[32,33] The transition state (TS) along the MEP is located via the climbing image (CI) implementation.[34] The MEP is calculated by a CI-NEB optimization where all degrees of freedom of H atoms and the first two Ag layers are fully relaxed while keeping the last three Ag layers at the DFT-bulk equilibrium positions. The stable endpoints of all CI-NEB calculations are allowed to relax to their respective local minima. These endpoints are connected through a set of images on the elastic band. The images are subsequently allowed to relax using a molecular dynamics minimization procedure in all degrees of freedom except for the direction of the band itself, until the forces and energy converge to the minimum energy path connecting the two endpoints. Harmonic vibrational frequencies of local minima and saddle points are calculated by diagonalizing the Hessian matrix, which is approximated via finite differences of forces, determined by displacing each center of the adsorbate by ±0.05 Å along each of the Cartesian coordinates.

Results

Chemisorption Sites. We investigated the stability of H on the Ag(111) surface using the DFT method. The relative stability of H adsorbed at symmetric sites was computed in a (2×2) surface unit cell corresponding to 0.25 ML. Four different sites of the Ag(111) surface were analyzed, namely the atop site (above an Ag atom), two three-hollow sites (between three Ag atoms), and a bridge site (between two Ag atoms). The calculated MEP for H diffusion connecting the symmetric sites is presented in Figure 1. The MEP is shown relative to the energy of hydrogen chemisorbed at the atop site. Adsorption of H on the atop site is energetically unfavorable by 11.2 kcal mol^{-1}, relative to the two three-hollow sites, (the fcc site above an Ag atom of the third layer, and the hcp site above an Ag atom of the second layer), which are energetically degenerate. Diffusion of H from an fcc to an hcp site through the bridge (TS in Figure 1) has an energy barrier of 2.7 kcal mol^{-1}. The small activation barrier between the energetically degenerate fcc and hcp sites suggests that H is highly mobile on the topmost layer of the Ag(111) surface at low surface coverage. Diffusion of H through the atop sites will be considerably slower, especially at low temperatures.

Lee and Plummer[24] have observed a dominant peak at 857 cm^{-1} using specular EELS spectra of H chemisorbed on the

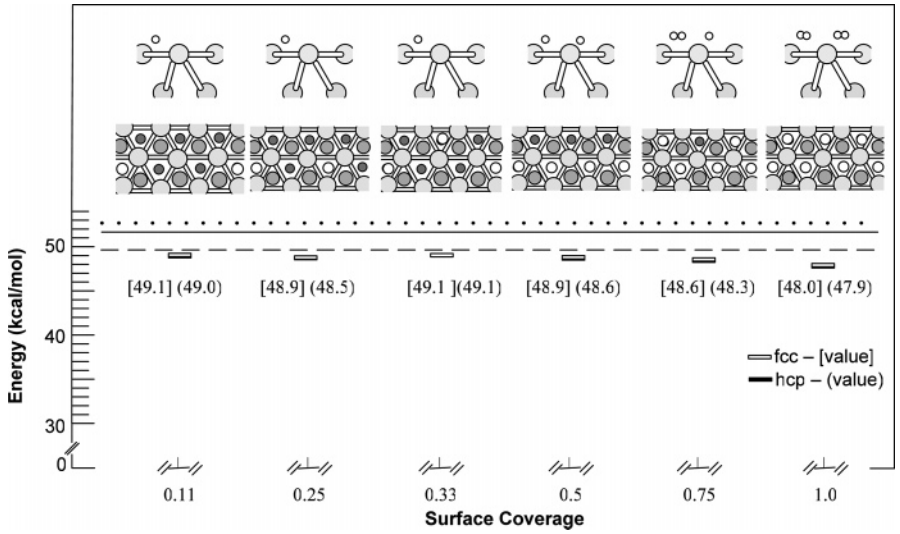

Figure 2. Coverage dependence of H binding energy to fcc sites on the Ag(111) surface. The results for the hcp sites are very similar, as shown by the numerical values below the data points, fcc [ ] and hcp ( ). The inset shows the molecular structures of H on the fcc sites of a subset of the Ag(111) surface. The horizontal solid, dotted, and dashed lines represent the experimental, uncorrected, and corrected ZPE DFT values of the H_2 binding energy per atom with numerical values of 51.63, 52.73, and 49.55 kcal mol^{-1}.

Ag(111) surface. The DFT-calculated harmonic frequencies of H on the *x*, *y*, and *z* direction of the fcc, hcp, and TS binding states are 783, 772, and 773; 736, 743, and 807; and 356*i*, 1059, and 969 cm^{-1}, respectively. The single imaginary frequency of the TS, represented with the letter *i*, shows the first-order character of the diffusion transition state. H frequencies on the fcc and hcp sites are underestimated by approximately 100 cm^{-1} compared with the experimental vibrational peak at 857 cm^{-1}.[24] The deviation can be attributed to the harmonic approximation that is used to calculate the theoretical vibrational frequencies. Considering this deviation, the experimental frequency is consistent with H being chemisorbed mainly to the three-hollow sites. The three-hollow site has been identified as the most energetically favorable adsorption configuration for H in other fcc(111) metals such as Ni(111), Pd(111), Pt(111),[2] and Cu-(111).[35] Thus, we have studied only the two three-hollow sites for H adsorption on the Ag(111) at different surface coverages.

Surface Coverage Dependence. The binding energy of H to the topmost layer of Ag(111) is calculated and reported with respect to the energy of a free hydrogen atom according to the equation

$$E_b^{H_{top}/Ag(111)} = -[E^{(Ag(111)+nH_{top})} - E^{Ag(111)} - nE^{(H)}]/n \quad \text{(E1)}$$

where n is the number of H atoms adsorbed per unit cell and the total energies of an isolated hydrogen atom, the bare silver slab and the hydrogen−silver system are represented by $E^{(H)}$, $E^{Ag(111)}$, and $E^{(Ag(111)\ +\ n\text{Htop})}$, respectively. By definition, a positive binding energy indicates that the desorption is endothermic.

The binding energies of H atoms to the two three-hollow sites are plotted in Figure 2, which includes a representation of the geometry of H on the fcc site. The data for fcc and hcp are essentially indistinguishable in the graph and are shown in text below the data points to highlight the fact that H is slightly more stable on the fcc site at all values of coverage. However, the largest energy difference between the two three-hollow sites is just 0.4 kcal mol^{-1}, which is within the accuracy of our calculations and is therefore only indicative. Overall, the stability of H on Ag(111) depends weakly on the surface coverage, falling in the 48−49 kcal mol^{-1} range below full monolayer. The decrease of 1.1 kcal mol^{-1} for H on the fcc site as coverage goes from 0.11 to 1.00 monolayer suggests a small repulsive H−H interaction on nonadjacent sites. It is difficult to predict the most stable H configuration that can be identified at low temperatures because of the similarities in the H stability at different surface coverages. The (1 × 1) LEED pattern has not been observed after H or D saturation on Ag(111); instead, a mixture of (2 × 2)/(3 × 3) LEED patterns has been observed at saturation coverage and the (2 × 2) and (3 × 3) LEED pattern are prominent at lower coverages.[15,24] The stability of the (2 × 2) and (3 × 3) facets are the most stable in our calculations. However, we cannot rule out the formation of the (1 × 1) facet after H saturation due to the small H−H repulsion at one ML. However, Figure 2 shows that the (1 × 1) facet is the least stable below one ML coverage. Therefore, we believe that the relative stability of the various systems are determined qualitatively well and our general understanding and conclusions of the H/Ag(111) system, especially at low coverages, will not be affected.

Our calculated values of the binding energy of H to the Ag(111) surface at different coverages to the different sites are slightly smaller than the binding energy of H in the H_2 molecule. Figure 2 shows horizontal lines representing the experimental, uncorrected, and DFT-corrected ZPE binding energies of H in the H_2 molecule with numerical values corresponding to 51.63 kcal mol^{-1}, 52.73 kcal mol^{-1}, and 49.55 kcal mol^{-1}, respectively. As observed, the binding energies of H to the surface are smaller than the binding energy of H in the H_2 molecule. Thus, the chemisorbed H atoms are unstable with respect to H in the H_2 gas molecule below one ML coverage. This is consistent with the observed instability of D atoms on Ag(111).[9,15] A recent study of H chemisorption on silver, using a nonperiodic 41-atom embedded cluster that represents the Ag(100) facet, found a binding energy of H of 42.7 kcal mol^{-1} in a hollow site at the configuration interaction (CI) level,[23] which brings theoretical support to the thermodynamic instability of H to the surface with respect to H in the gas-phase H_2. The weak interaction of H to Ag(111) has been associated with the observation of the H 1s antibonding overlap situated below the Fermi energy level of the experimentally recorded density of states of the H-covered Ag(111) surface.[36] This observation is consistent with the d-band model in which the hybridization of the H 1s state with the d band of the noble metal results in the formation of

TABLE 1: Variation of the Coverage Dependence of Structural Parameters for Chemisorption of H on an Ag(111) fcc Site[a]

coverage	structural parameters for H on the fcc site			
θ	d(Ag−H)	r(Ag−H)	d_{12}	d_{23}
1.00	0.7985	1.9252	2.5061	2.4068
0.75	0.8500	1.8510	2.4786	2.3907
0.50	0.8691	1.8772	2.4428	2.4026
0.33	0.8798	1.9104	2.3998	2.3794
0.25	0.8688	1.9076	2.4102	2.3787
0.11	0.8954	1.9140	2.3969	2.3738

[a] The Table shows the distances above the surface of H to the center of mass of the topmost Ag layer, d(Ag−H), the shortest Ag−H bond distance, r(Ag−H), and the Ag interlayer distances (all in Å).

a bonding and antibonding adsorbate−metal d state largely occupied below the Fermi energy level preventing a strong covalent bonding interaction,[37] which is consistent with our calculated DFT-projected density of states provided as Supporting Information of hydrogen chemisorbed on the Ag(111) surface.

Equilibrium structural parameters of H chemisorbed to the topmost Ag layer of the Ag(111) surface are presented in Table 1. The vertical height of H atoms to the center of mass of the first Ag layer, d(Ag−H), the bond length of H to the nearest Ag atom, r(Ag−H), and the interlayer distances between the center of mass of the first and second layers, d_{12}, and between the second and third layers, d_{23}, are shown. The structural parameters are given for the fcc site as an example, but the structural differences between H on fcc and H on hcp sites are very small. Bound H is found to be at d(Ag−H) = 0.89 Å above the surface at 0.11 ML, and the distance to the surface changes by a maximum of 0.1 Å when the surface is populated by H atoms. Small changes in the equilibrium d(Ag−H) distance, by less than 0.04 Å at 0.33 ML, for instance, do not lead to changes in the binding energy, suggesting a flat energy surface near equilibrium. The second interlayer distance (d_{23}) is almost unperturbed over the range of surface coverage studied. The first interlayer distance (d_{12}) is modestly expanded compared with the equilibrium DFT-bulk interlayer distance (d_{DFT} = 2.3902 Å) in the presence of H on the surface, reaching a maximum of 4.9% expansion at full monolayer. In contrast to the behavior for d_{12}, the vertical height of H atoms to the center of mass of the first Ag layer d(Ag−H) decreases as the surface coverage increases; the closer the interaction of H atoms with the first Ag layer, the larger the expansion of the d_{12} interlayer distance.

The work function change ($\Delta\phi$) induced by the adsorption of H to the Ag(111) surface has been measured experimentally. Zhou et al.[12] found that adsorbing D atoms on the Ag(111) surface caused a decrease in $\Delta\phi$ by 0.17 eV at saturation. However, more recent works by Lee and Plummer[24] and by Zhukov et al.[38] show a maximum increase in $\Delta\phi$ by 0.32 and 0.24 eV, which were obtained at maximum H coverages of 0.6 and 0.65 ML, respectively. The DFT-calculated work function change ($\Delta\phi_{DFT}$) induced by the adsorption of H atoms to the Ag(111) surface at different coverages in the two three-hollow sites are depicted in Figure 3. The average of the work function of the different bare Ag unit cells is calculated to be 4.49 eV, in good agreement with the experimental work function of Ag of 4.46 eV.[39] It can be seen in Figure 3 that the $\Delta\phi_{DFT}$ increases almost linearly upon saturation of the Ag(111) surface with H atoms, reaching a maximum value of 0.45 eV at one monolayer indicating the formation of a dipole layer. The sign of the $\Delta\phi_{DFT}$ is always positive. The magnitude of $\Delta\phi_{DFT}$ is small but a bit larger than that for other H/metal systems,[2] possibly because of a combination of the charge transfer from Ag(111) to chemisorbed H and the expansion of the d_{12} layer as the surface coverage increases as observed in Table 1.

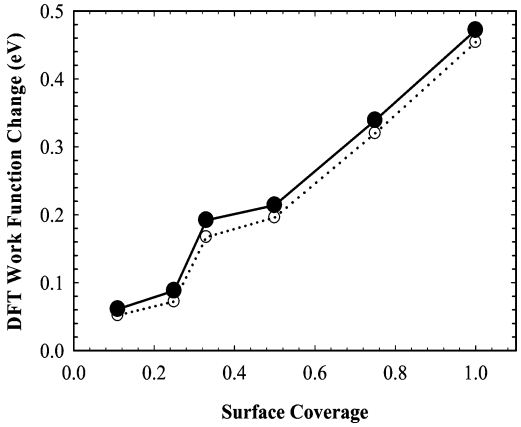

Figure 3. Coverage dependence of the H-induced work function change, $\Delta\phi_{DFT}$, with respect to the surface coverage in the fcc sites (open circles) and hcp sites (filled circles) of the Ag(111) surface.

H Chemisorption at Vacancy and Subsurface Sites. When silver is reacted with oxygen-containing H species at high temperatures, microscopic "pinholes" in the surface structure are formed. It has been postulated that chemical reactions at subsurface sites of Ag(111) create these pinholes by displacing Ag atoms from their equilibrium positions when molecules desorb to the gas phase, for instance, desorption of subsurface water to the gas phase over 600 °C.[40−42] To gain insight into the role of hydrogen in point defects of the Ag(111) surface, we have computed the binding energy of H at vacancies.

The binding energy of H at a vacancy of the Ag(111) surface is calculated and reported with respect to the energy of a hydrogen atom according to the equation

$$E_{b-vac}^{H/Ag(111)} = -[E^{(Ag(111)\_vac + nH)} - E^{Ag(111)\_vac} - nE^{(H)}]/n \quad \text{(E2)}$$

where the total energies of the silver slab with a vacancy in the topmost layer and the hydrogen−silver system are represented by $E^{Ag(111)\_vac}$ and $E^{(Ag(111)\_vac\ +\ nH)}$, respectively.

A single hydrogen atom was placed at each vacancy, and the system, including the first two Ag layers, was fully relaxed. Figure 4 shows the binding energies of H at vacancy sites using the (3 × 3), (2 × 2), and ($\sqrt{3}$ × $\sqrt{3}$)R30 unit cells together with horizontal lines representing the experimental, uncorrected, and corrected ZPE binding energies of H in the H_2. We found that H is chemisorbed at the three-hollow sites between the first and second Ag layers in the center of the vacancy as depicted in the inset of Figure 4. The binding energy of H to an existing vacancy, $E_{b-vac}^{H/Ag(111)}$, decreases slightly from 42.6 kcal mol^{-1} using the (3 × 3) unit cell to 40.8 kcal mol^{-1} using ($\sqrt{3}$ × $\sqrt{3}$)R30. A similar trend was also found for H at the topmost layer. A normal-mode analysis shows that H at the vacancy site in the (2 × 2) unit cell is a minimum structure with frequencies of 129, 109, and 94 cm^{-1}.

We also calculated $E_{b-vac}^{H/Ag(111)}$ by moving the H atom to the edges of the vacancy using the (2 × 2) unit cell. We found an H atom in equilibrium at d(Ag−H) = 0.9535 Å below the center of mass of the first layer, above an Ag atom of the third layer. The binding energy in this location is$E_{b-vac}^{H/Ag(111)}$ = 38.3 kcal mol^{-1}, which is 2.9 kcal mol^{-1} lower than the binding energy of H at the center of the vacancy. Note that $E_{b-vac}^{H/Ag(111)}$ at the

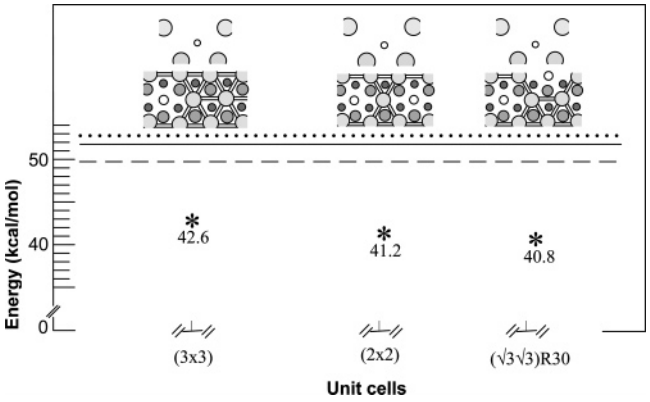

Figure 4. Coverage dependence of H binding energy to an existing vacancy site of the Ag(111) surface, $E_{b-vac}^{H/Ag(111)}$. The numerical values of the binding energy are shown in the Figure. The inset shows a side and top view of the molecular structures of H to the vacancy site. The horizontal solid, dotted, and dashed lines represent the experimental, uncorrected, and corrected ZPE DFT values of the H_2 binding energy per atom with numerical values of 51.63, 52.73, and 49.55 kcal mol^{-1}.

TABLE 2: Adsorption Properties of H at Vacant Sites in Ag(111)[a]

unit cell	$E_{rem}^{Ag/Ag(111)}$	$E_{b-vac}^{H/Ag(111)}$	$E_{sub}^{H/Ag(111)}$	d(Ag−H)	d	d_{23}
0.33	9.2	40.8	33.3	−1.5257	2.3240	2.4110
0.25	10.8	41.2	30.4	−1.5578	2.3952	2.4018
0.11	13.0	42.6	27.8	−1.5574	2.3666	2.3920

[a] The binding energy at a vacancy, $E_{b-vac}^{H/Ag(111)}$, the substitutional energy of hydrogen for an Ag atom, $E_{sub}^{H/Ag(111)}$, and the removal energy of Ag from the top layer, $E_{rem}^{Ag/Ag(111)}$, are given in kcal mol^{-1}. The distance of the H atom to the center of mass of the first layer, d(Ag−H), and the surface interlayer distances, d_{12} and d_{23}, are given in Å. The binding energy of H to the vacancy, $E_{b-vac}^{H/Ag(111)}$ and the energy to substitute and Ag atom, $E_{sub}^{H/Ag(111)}$, are calculated with respect to the energy of an H atom.

center of the vacancy is ∼8−9 kcal mol^{-1} smaller than the binding energy of H at the topmost layer in the range of surface coverage studied. The binding energy of hydrogen at different positions of the vacancy is lower than the binding energy of H to the H_2 molecule. If hydrogen atoms are chemisorbed at a vacancy, then recombination of H inside a vacancy to form H_2 would be an exothermic process and formation of H islands at vacancies would be thermodynamically unstable.

The energy involved for H to substitute for a single Ag atom in the Ag(111) system was also calculated. The substitutional adsorption energy is calculated as defined by Scheffler and Stampfl[43]

$$E_{sub}^{H/Ag(111)} = -[E^{(Ag(111)\_vac+nH)} + nE^{Ag-bulk} - E^{Ag(111)} - nE^{(H)}]/n \quad \text{(E3)}$$

where each substituted Ag atom is presumed to be re-adsorbed at a kink site after removal and to contribute $E^{Ag-bulk}$, to the substitutional energy balance. For the present calculations, only a single vacancy substitution is analyzed. The energy required to form a vacancy, namely by moving an Ag atom in equilibrium with the topmost layer to a kink site, $E_{rem}^{Ag/Ag(111)}$, is calculated as the difference between $E_{b-vac}^{H/Ag(111)}$ and $E_{sub}^{H/Ag(111)}$. A positive number for the removal energy represents an endothermic process.

Table 2 summarizes the adsorption properties of H at the vacancy sites of Ag(111). As can be seen, the vacancy formation is an endothermic process, as expected, in the range of ∼10−13 kcal mol^{-1}. The removal of an Ag atom from its equilibrium position produces an inward relaxation of the first interlayer distance of the Ag(111) surface by 1.7% in response to the vacancy formation. The second interlayer distance is almost unaltered by the vacancy formation. The substitution of Ag by H in the Ag(111) surface is 28−33 kcal mol^{-1} exothermic as defined by eq E3. This relatively low value arises because the Ag removal energy from the equilibrium lattice is a significant fraction of the H binding energy at the vacancy. The equilibrium position of H at the vacancy is found to be ∼1.5 Å below the first layer and ∼0.8 Å above the second layer. There is an inward relaxation of the d_{12} interlayer distance and slightly expansion of the d_{23} with respect to the DFT-bulk interlayer distance, as seen in Table 2.

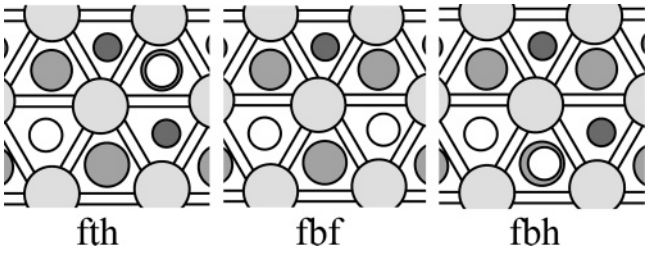

Figure 5. Geometry representation of H binding states on the Ag(111) surface at 0.5 ML. The Ag(111) surface geometry is represented in gray with the largest circles showing the Ag atoms on the topmost layer. Hydrogen is shown with small white circles.

With respect to the existence of subsurface hydrogen when there are no vacancies in the silver structure, we tested the subsurface sites that can locate H atoms that migrate directly from the topmost layer. We have examined the octahedral and tetrahedral sites that are located below the fcc and hcp sites, respectively, between the first and second layers. We found that no H atoms can reside in subsurface sites (specifically, between the first and second Ag layers) when the surface coverage is below 0.75 ML. Any attempt to optimize bulk hydrogen below this surface coverage was unsuccessful with the H atom(s) being pulled up to the topmost layer. At 1 ML surface coverage, however, a subsurface hydrogen atom is found in the octahedral and tetrahedral sites with a binding energy to the surface of 39.40 and 40.85 kcal mol^{-1}, respectively, calculated using eq E1. Hydrogen is in equilibrium closer to the topmost layer rather than to the second Ag layer, being ∼2.0 Å above the second layer and 0.7647 and 0.8168 Å below the first layer in the octahedral and tetrahedral sites, respectively. The binding energies at these subsurface sites are approximately 8 kcal mol^{-1} lower than the binding energies at the topmost layer and, in all cases, lower than the binding energy of H in the H_2 molecule. Therefore, diffusion of H from top sites to subsurface sites is a highly endothermic process. This is consistent with experimental evidence that hydrogen saturates below monolayer coverage, in which case no hydrogen diffuses to subsurface sites.[24]

Minimum Energy Paths of H Reactions on the Ag(111) Surface. We determined different binding states of H pairs to compare directly the stability of different ordered structures at 0.5 ML, as shown for the most stable configurations in Figure 5. The two most stable states are nearly degenerate, each comprising H atoms in three-hollow sites. The slightly more stable structure (fth in Figure 5) binds the H atoms at distant fcc and hcp sites; the H atoms are located 0.92 Å above the center of mass of the topmost layer with an H−H distance of 3.39 Å. The second, nearly degenerate H structure is found 1.0 kcal mol^{-1} above the fth state; the H atoms are bound on fcc sites (fbf in Figure 5) and are located 0.86 Å above the center of mass of the topmost layer with an H−H distance of 2.93 Å. A

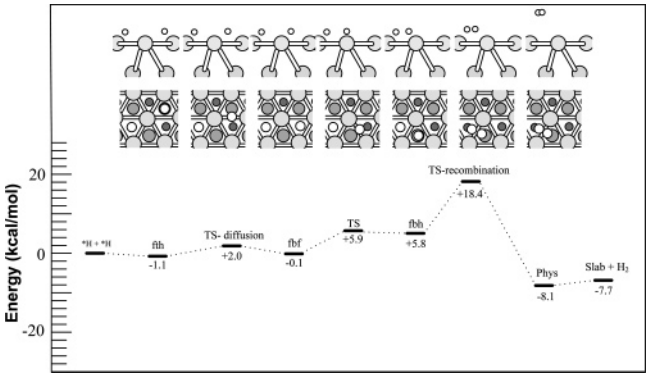

Figure 6. Minimum energy path (MEP) at 0 K; with no zero point energy correction to the electronic energy; of H diffusion and recombination through the bridge sites of the Ag(111). The MEP is plotted with respect to H chemisorbed at infinite separations. Transition states are represented with TS. The inset shows a top and side view of H to the Ag(111) surface.

TABLE 3: Relevant Information of H Binding States at Half Monolayer[a]

species	r(H−H)	d(Ag−H)	d_{12}	d_{23}
fbh	2.2248	H_{fcc}= 0.8580, H_{hcp}= 0.8661	2.4385	2.3659
fbf	2.9280	H_{fcc}= H_{fcc}= 0.8609	2.4533	2.3909
fth	3.3857	H_{fcc}= 0.9025, H_{hcp}= 0.9362	2.4361	2.3580
TS diffusion	3.0761	H_{fcc}= 0.8527, H_{bridge}= 1.1081	2.4351	2.3712
TS	2.3563	H_{fcc}= 0.8673 H_{bridge}= 0.9762	2.4404	2.3737
TS recombination	1.1918	H_{fcc}= 1.0414, H_{hcp}= 1.0492	2.4363	2.4009

[a] The Table shows the distance between H atoms, r(H−H), the distance of the H atoms to the center of mass of the topmost Ag Layer, d(Ag−H), the first two Ag interlayer distances, d_{12} and d_{23}, taken as the difference in the center of mass, and the harmonic frequencies. Distances are given in Å, and frequencies are given in cm^{-1}.

metastable state occurs when the H atoms are bound on neighboring fcc and hcp sites (fbh in Figure 5). The fbh energy is 6.9 kcal/mol above that of the fth structure; the H atoms are 0.86 Å above the surface with H−H distance of 2.20 Å. The energetics of the binding states reveals small long-range H−H interactions and considerable repulsive interactions at neighboring sites.

The minimum energy paths (MEP) of H diffusion and recombination to H_2 on the topmost layer of the Ag(111) surface were examined from the H binding states at 0.5 ML. Recombination of H to H_2 may occur from the H binding states directly, namely on the atop site as from the fth binding state; on the bridge site as from the fbf binding state, and on the hollow site as from the fbh binding state. Calculation of the transition state of the direct H−H recombination from the fth binding state could not be achieved because the CI-NEB band moves toward the bridge site as the optimization proceeds. This is mainly because of the weak interaction of H with the atop site as observed in Figure 1. The energy barrier of H−H recombination from the fbf binding state is 7.4 kcal mol^{-1} larger than the energy barrier for H−H recombination from the fbh binding state. Therefore, H diffuses from the fth binding state before H−H recombination takes place. Figure 6 shows the MEP (without zero point energy correction to the electronic energy) of H diffusion and H−H recombination on the Ag(111) surface. Selected optimized geometrical parameters of surface species are shown in Table 3. The energy values of the MEP are calculated relative to the energy of 2 × H chemisorbed at large separation, namely, relative to the energy of two single H chemisorbed on fcc sites in separated unit cells. The final state of the MEP is represented by the energy of the isolated H_2 molecule plus the energy of the bare slab.

We found that recombination of H to H_2 is an exothermic activated process. As can be seen in Figure 6, diffusion of H on the Ag(111) through the bridge sites has a low energy barrier while H−H recombination has a relatively high energy barrier. Diffusion of H from a nonadjacent hcp site to an fcc site, namely, from fth to fbf, has an energy barrier of 3.1 kcal mol^{-1} with the top of the barrier corresponding to the location of the H atom above a bridge site. The reverse barrier is 2.1 kcal mol^{-1}. A further diffusion of H from an fcc site to an adjacent hcp site, namely, from fbf to fbh, has an energy barrier of 0.1 kcal mol^{-1} above the 5.9 kcal mol^{-1} endothermicity of the reaction. Recombination of H from adjacent sites is activated with an energy barrier of 12.6 kcal mol^{-1}. The H−H center of mass of the recombinative transition state is located 1.0 Å above the center of mass of the topmost layer. The H−H bond length at the recombinative saddle point is 60% longer than the equilibrium DFT H_2 bond length. There is still a considerable interaction between hydrogen and the surface at the saddle point, which is characteristic of a late H_2 dissociation transition state. This is consistent with different dynamics studies on noble metal surfaces[44] and specifically with experimental observations of the vibrational enhancement of D_2/H_2 dissociation on the Ag(111) surface.[10,45]

No molecular chemisorbed H_2 is found in equilibrium with the Ag(111) after H recombination. Moving the H−H species away from the topmost layer leads to the formation of a physisorbed H_2 state, which, after full optimization for a local minimum, stands at a distance of ∼3.8 Å above the Ag(111) surface. The physisorption energy of H_2 is calculated to be 0.4 kcal mol^{-1}. We found the H_2 physisorption energy to be independent of molecule orientation, behaving as a free rotor. Although DFT does not describe dispersion forces properly, the predicted adsorption energy shows that the interaction of $H_{2(g)}$ with Ag(111) is very small. The physisorbed state of H_2 on Ag(111) has been observed experimentally using diffractive selective adsorption (DSA)[46] and HREELS.[5] From these studies, it is deduced a weakly bound $H_{2(g)}$ molecule to the Ag(111) surface, consistent with our DFT-GGA calculations. The small magnitude of the physisorption energy and the absence of a pronounced energy barrier for its desorption implies that physisorbed hydrogen will have an extremely short lifetime and that it will have no significant effects on the kinetics of H recombination.

The total energy gain after reaching the H−H recombination transition state to form an H_2 molecule is 26.1 kcal mol^{-1}, in good agreement with the DFT energy barrier calculated for dissociation of H_2 on Ag(111).[20] The large DFT-predicted energy gain is consistent with the experimentally observed nondissociative chemisorption of H_2 on Ag(111) below 100 K.[9] Eichler et al.[21,22,47] have calculated an H_2 dissociation barrier larger than 25 kcal mol^{-1} on the Ag(100) facet and the pronounced barrier for the H_2 entrance channel seems to be the pattern for dissociation on Ag surfaces.

The total H−H recombination energy barrier calculated from the fbf binding state is 18.5 kcal mol^{-1}. Considering the metastable character of the adjacent H−H configuration (fbh), this can be compared with the activation energy deduced from analysis of TPD spectra (6.5−10.5 kcal mol^{-1}). The difference between the experimental and DFT-GGA barrier is larger than the expected errors associated with the DFT formalism. Because the maximum rate of H_2 desorption occurs below 200 K in TPD experiments, the penetration of H atoms through the H recombination barrier due to quantum tunneling effects could

TABLE 4: Harmonic Frequencies, ν_i , in cm^{-1} and Zero Point Energy (ZPE) in kcal mol^{-1} of H−Ag(111) Binding States[a]

binding state	frequencies	zero point energy
fth	747, 742, 846, 819, 809, 808	6.82
TS diffusion	1142, 333*i*, 1009, 798, 807, 827	6.55
fbf	974, 860, 688, 741, 803, 803	6.96
TS recombination	1270*i*, 294, 528, 698, 880, 864	4.67
H_2	4450	6.36

[a] The imaginary frequency of the transition state is shown with the letter *i*. The ZPE is calculated as $\sum_i(1/2)hc\nu_i$ excluding the absolute value of the imaginary frequency for transition states in kcal mol^{-1}

be significant. Therefore, we have estimated the effect of quantum tunneling in the rate of H−H recombination reaction.

Reaction Rates. The rate of hydrogen diffusion and recombination were calculated using transition state theory (TST). The temperature-dependent rate constant was calculated according to the equation

$$k_{TST}(T) = \frac{k_B T}{h}\frac{Q_{TS}}{Q_{IS}}\exp(-\Delta E/RT) \qquad \text{(E4)}$$

where ΔE is the zero point corrected energy barrier, Q_{TS} and Q_{IS} are the partition functions for the transition state and initial state, respectively, k_B is Boltzmann's constant, h is Plank's constant, T is the temperature, and R is the universal gas constant. The total partition functions of the various surface species (local minima and transition states) were calculated using the vibrational and frustrated translational frequencies, ν_i (tabulated in Table 4) according to the equation

$$Q_{surface-species} = \prod_i \frac{1}{1-\exp(-ch\nu_i/k_B T)} \qquad \text{(E5)}$$

where c is the speed of light. Partition functions were computed in the temperature range 140−1100 K in steps of 20 K. Experimental evidence suggests that surface reactions that involve hydrogen atoms can undergo quantum tunneling effects that increase the reaction rate.[48] The classical description of the TST theory as shown in eq E4 does not account for quantum effects that might affect the reaction rate. Quantum tunneling effects in the H/Ag system were considered in this study by computing the transmission coefficient due to penetration of hydrogen through the barrier only in the degree of freedom corresponding to the reaction coordinate. It is important to note, however, that for the H_2/Cu(111) system it has been shown that a low-dimensional treatment overestimates the transmission coefficient compared to a high-dimensional treatment.[49] The tunneling correction was calculated by generating an Eckart potential[50] from the MEP corrected for DFT zero point energy, treating the imaginary frequency of the transition state as a real number. The temperature-dependent Eckart transmission coefficient ($\Gamma(T)_{Eckart}$) was calculated numerically according to the equation[50]

$$\Gamma(T)_{Eckart} = \exp(\Delta E/RT)\int_0^\infty \exp(-E/RT)\,k(E)\,d(E/RT) \qquad \text{(E6)}$$

where $k(E)$ is the permeability function that describes the probability that chemisorbed H atoms with energy E cross the barrier to the products side, namely H_2(g). The permeability was calculated from an energy $E = 0$ to an energy value well above the energy barrier from $E = 0$ kcal mol^{-1} to $E = 80.5$ kcal mol^{-1} according to the equation

$$k(E) = 1 - \frac{\cosh(2\pi(\alpha-\beta)+\cosh[2\pi\gamma]}{\cosh(2\pi(\alpha+\beta)+\cosh[2\pi\gamma]} \qquad \text{(E7)}$$

where $\alpha = 0.5\sqrt{E/C}$, $\gamma = 0.5\sqrt{(b-C)/C}$, $C = (hc\nu^{\ddagger})^2 b/16\Delta E'(\Delta E' - \Delta H')$, $b = (2\Delta E' - \Delta H') + 2[\Delta E'(\Delta E' - \Delta H')]$, and $\beta = 0.5\sqrt{(E-\Delta H')/C}$. The parameters $\Delta E'$ and $\Delta H'$ are the energy barrier and heat of reaction derived from the Eckart potential. The Eckart tunneling correction has been used in other heterogeneous catalytic system studies, such as the C−H cleavage of methane over Pd(111) where a significant tunneling effect is observed and that brings the theory in better, but not fully, quantitative agreement with experiments.[51] For comparison purposes, we have also calculated the transmission coefficient using the Wigner formalism[52] for which the transmission coefficient depends only on the imaginary frequency at the saddle point and not on the thermodynamics of the reaction.

$$\Gamma(T)_{Wigner} = 1 + \frac{1}{24}(hc\nu^{\ddagger}/k_B T)^2 \qquad \text{(E8)}$$

As shown in Table 4, the diffusion and recombination transition states each contain a single imaginary frequency, which is characteristic of first-order transition states. The absolute value of the imaginary frequency of the diffusion transition state is small, suggesting a flat potential near the transition state. The diffusion energy barrier (taken from fth to TS diffusion) is small and unlikely to be strongly influenced by quantum tunneling effects. However, the imaginary frequency of the recombination transition state is large, suggesting considerable curvature of the potential energy surface at the saddle point. The energy barrier between fbf and TS recombination is relatively high, and the recombination rate constant is therefore more likely to be strongly affected by tunneling effects.

The Arrhenius plots (Ln(k) vs 1/T) of the H recombination rate constants with and without tunneling corrections are plotted in Figure 7 and numerical values of the Wigner and Eckart tunneling factors at selected temperatures are shown in Table 5. The recombination rate constant was calculated using the local minimum fbf as the initial state and the TS recombination as the saddle point. Tunneling corrections to the recombination rate from the minimum fbf take into consideration possible recombination of H_2 through the fth binding state. It can be seen in Figure 7 that tunneling corrections to the rate constant are negligible at high temperatures but become important at low temperatures, as expected.

The Wigner correction often grossly underestimates the tunneling effect because it only accounts for contributions near the top of the barrier, and this appears to be the case here at lower temperatures where, as shown in Table 5, the Wigner transmission coefficient is much smaller than the Eckart value. The Eckart transmission coefficient tends to overestimate the tunneling factor especially at low temperatures when the approximate Eckart potential contains a narrower width than the real one.[53] However, the Eckart transmission coefficients, although with some errors, are certainly a good approximation of the exact tunneling contributions to the rate constant as exemplified in the hydrogen exchange reaction H + H_2 in the gas phase[54] and has been used to provide an adequate interpretation of experimental data on the C−H cleavage of saturated hydrocarbons by transition metals.[55,56] In our case, the calculated enhancement of the recombination rate due to the quantum tunneling effects predicted by the Eckart formalism is a factor of 1691 at 200 K. Clearly, low-temperature H recombination on Ag(111) is driven by tunneling and the effective barrier is

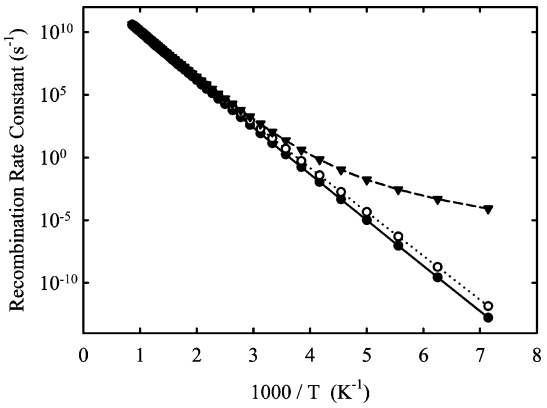

Figure 7. DFT-calculated H recombination rate constant at 0.5 ML in the temperature range of 140 K to 1100 K on Ag(111). Data points represent the calculated values, and the lines show parametric fits to these (see the text and Table 6). Filled circles represent the classical transition-state rate constant without tunneling correction; the opened circles represent the Wigner-corrected values, while the filled triangles represent the Eckart-corrected rate constant.

TABLE 5: Numerical Values of the Wigner and Eckart Transmission Coefficients Γ(T) for H Recombination Reaction on the Ag(111) Surface

	temperature (K)					
	200	240	260	300	500	1000
Γ(T) Wigner	4.5	3.4	3.1	2.5	1.6	1.1
Γ(T) Eckart	1691.7	59.8	23.9	8.1	1.9	1.2

significantly lower than the saddle point energy. The strong effect of tunneling at lower temperatures leads to a curved Arrhenius plot. Such curvature has been interpreted previously as a manifestation of tunneling, especially for large activation barriers and large curvature of the potential energy surface.[57]

Simulation of Temperature Program Desorption Profiles. On the basis of the MEP discussed above, we can simulate the adsorption/desorption behavior of H_2 via the following elementary steps

$$2H^* \rightleftharpoons H^*-H^*_{fth} \quad \text{(R1)}$$

$$H^*-H^*_{fth} \rightleftharpoons H^*-H^*_{fbf} \quad \text{(R2)}$$

$$H^*-H^*_{fbf} \rightarrow H_{2(g)} + 2^* \quad \text{(R3)}$$

Here a surface site is represented by *. The diffusion reactions (R1−R2) are allowed to take place in the forward and reverse directions with heats of reactions at 0 K including the zero point energy of −1.0 and +1.2 kcal mol^{-1} while the recombination reaction (R3) is allowed to take place in the forward direction only. The chemisorption of $H_{2(g)}$ molecules is suppressed. The rate constant for reaction R1, namely, the diffusion of two chemisorbed H at infinite separation, is approximated as the diffusion of a single H atom. The H diffusion rate constants, namely, R1 and R2, are calculated with no tunneling corrections as the energy barrier and the imaginary frequency of the transition states are very small, making the tunneling corrections negligible. We have used the classical TST to calculate the diffusion rate constants, but variational TST should be used if more accurate results are desired. For the present simulations, we observe that diffusion is not the rate-determining step during the H_2 desorption process and that classical TST is appropriate. The rate constants are all evaluated at 0.5 ML.

The rate constants are expressed in terms of the three-parameter Arrhenius form:

$$k_f = AT^n \exp(-E_a/RT) \quad \text{(E9)}$$

The three parameters were calculated using a least-squares minimization procedure taking as a reference the rate constant derived from the first-principles calculations. The rate constant R3 with tunneling could not be fitted satisfactorily to a single set of Arrhenius parameters because of the curvature of the Arrhenius plot at low temperatures. Therefore, we described this reaction as two parallel reactions, one dominant at high temperatures and the other dominant at low temperatures. The rate constant parameters are shown in Table 6.

The harmonic frequencies given in Table 4 are used to calculate polynomial expressions for heat capacity, entropy, and enthalpy for surface species that are used in the simulation of the TPD profiles, specifically for the calculation of equilibrium constants and reverse rates for each step. The thermodynamic data for gas-phase hydrogen was taken from the literature.[18] We have used a site density of 4.58×10^{-9} mol cm^{-2}, which is calculated from the surface atom density of Ag(111) (1.38×10^{15} cm^{-2}) and the number of sites per surface atom. All kinetic simulations were carried out using the Chemkin suite.[58]

The simulated TPD profiles using the rate constants with and without tunneling corrections are compared to two sets of published experimental results in Figure 8. There are a range of experimental TPD data available in the literature for hydrogen and deuterium on Ag(111), and we selected studies that represent the lower and upper limit for the temperature at which the H_2 desorption rate peaks appear. Curves a and b in Figure 8 show experimental data obtained for TPD of an initial saturation coverage of H on Ag(111). Zhukov et al.[38] observed the H_2 desorption peak at 164 K using 3 K s^{-1} (curve a) while Zhou et al.[12] observed an H_2 desorption peak at 191 K with a heating rate of 4 K s^{-1} (curve b). The wide range of desorption temperatures has been ascribed to different levels of surface roughness.[38]

It can be seen in Figure 8 that the predicted TPD desorption peak occurs at higher temperatures than is observed experimentally. The predicted location of the TPD peak is at 289 K using the classical rate constant parameters (curve d) and at 264 K when tunneling is included via Eckart correction in R3 (curve c). The Eckart tunneling factor to the classical rate constant decreases the TPD peak by 25 K. The TPD peak with Eckart tunneling corrections is 100 and 73 K higher than the experimental TPD peaks (curves a and b). We find that the location of the H_2 desorption peak in the models is insensitive to the thermodynamics and kinetics of the diffusion reactions and depends only on the rate of recombination which is, in turn, most sensitive to the activation energy for the process, especially at lower temperatures. The discrepancy between the experiments and the theory can be expressed as a change in the apparent activation energy for recombination needed to bring the theory and experiment into alignment. As shown by the error bars in Figure 8, the TPD with Eckart tunneling is relatively more sensitive to the change of activation energy than the classical TST. Reducing the apparent activation energy for recombination (with Eckart tunneling correction) by 3.1 kcal mol^{-1} shifts the peak to encompass the full range of experimental values. By way of comparison, if we use the classical value without tunneling correction, a reduction in the apparent activation energy of some 5 kcal mol^{-1} would be needed to cover the range of experimental data. A decrease of a few kcal mol^{-1} in the energy barrier is consistent with the likely uncertainty of the PW91 density functional that overpredicts the H binding energies. However, a recent theoretical study reported that the

TABLE 6: Transition State Rate Constant Parameters Expressed as $k = AT^n \exp(-E_a/RT)$ for H Diffusion and Recombination to H_2 on Top of the Ag(111) Surface[a]

reaction	TST	*A*	*N*	E_a
R1	$k_{TST}^{clasical}$	3.66×10^{12}	0.18	2.59
R2	$k_{TST}^{clasical}$	5.80×10^{12}	0.11	3.28
R3	$k_{TST}^{clasical}$	3.16×10^{10}	1.04	16.35
	k_{TST}^{Eckart}	3.95×10^{3}	3.09	12.58
		7.08×10^{-1}	1.57	4.75

[a] The Table shows the rate constant for H recombination (R3) with and without the Eckart correction for tunneling. The apparent activation energy (E_a) is given in kcal mol^{-1}, and the pre-exponential factor (*A*) is given in s^{-1}.

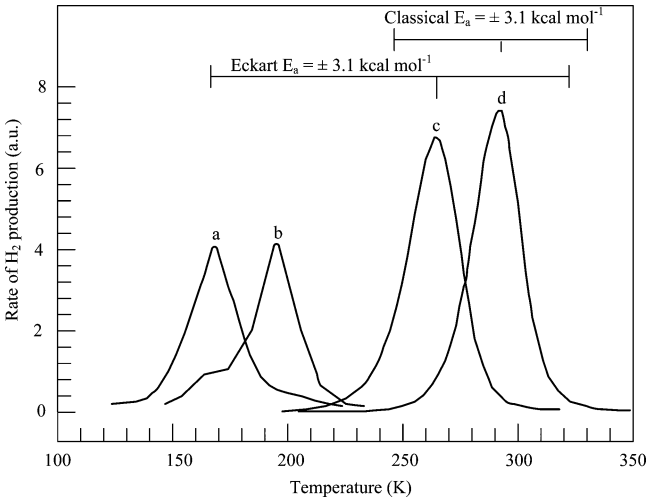

Figure 8. Temperature program desorption profiles of H_2 from an H covered Ag(111) surface. Profiles a and b are experimental values taken from refs 38 and 12, respectively. Profiles c and d are predicted values using Eckart-corrected rate constants and classical TST rate constants, respectively, using heating rates of 3 K s^{-1}. Values from ref 12 were multiplied by 4 in order to compare peak positions. The peak positions for profiles a, b, c, and d are 164, 191, 264, and 289 K, respectively.

RPBE density functional predicts rather higher energy barriers than the PW91 density functional for H−H dissociation on Ru(0001).[59] We have recalculated the energy barrier for H−H recombination on Ag(111) as expressed in reaction R3 using the RPBE functional. For our system, the RPBE barrier is just 0.4 kcal mol^{-1} higher than that found using the PW91 functional.

Although our first-principles results do not describe the experimental results in their entirety, we can conclude based on the calculated ab initio energy barrier that quantum tunneling of H through the recombination barrier to form H_2 on the Ag(111) surface has a significant effect on the H_2 temperature of desorption due to the low temperatures at which it occurs. The discrepancy between experiment and theory may be resolved by reducing the activation energy of recombination by a maximum of ~3 kcal mol^{-1} after an Eckart tunneling correction is applied. The origin of this difference might be associated with an underestimation of the effect of the coupling between other molecular and surface degrees of freedom during recombination. Of particular importance is the dynamic coupling with the lattice surface that is not included in our kinetic study and that may have a particular importance for this system. A justification for this view is the experimental observation of a substrate activation assisted desorption process of $D_{2(g)}$ from Ag(111).[60] Describing the H/Ag system solely by a static ab initio MEP suppressed the dynamic coupling of the degrees of freedom of the adsorbate with the Ag(111) surface, which has been important in elucidating the diffusion constant of hydrogen[61,62] and the difference between experimental activation energy and ab initio energy barriers for C−H cleavage of CH_4 on metal surfaces,[63,64] for instance. It is obvious from the difference in the temperature of desorption from the TPD profiles that the activation energies deduced from experiments are only apparent and are not related in any simple way to the ab initio barrier height. High-dimensional dynamic analysis of the H/Ag(111) surface is necessary to quantify the effect of surface temperature and translational energy of H_2 to the rate of reaction.

Conclusions

Chemisorbed H atoms are unstable with respect to the H_2 molecule in all adsorption sites of the Ag(111) below 1 ML. The binding energy of H to the surface decreases slightly with increasing surface coverage below one monolayer, suggesting a small repulsive H−H interaction on nonadjacent sites. Desorption of H_2 from chemisorbed H atoms is an activated and exothermic process. The H_2 desorption is rate-limited by recombination because the H diffusion has a very low energy barrier. The permeability of H atoms through the recombination energy barrier is large at low temperatures, increasing the rate constant of H_2 desorption due to quantum tunneling effects.

Acknowledgment. We acknowledge the support of the Australian Research Council and the Australian Partnership for Advanced Computing. A.S. acknowledges the support provided by an Australian Postgraduate Award and by Heatric, a division of Meggitt U.K. A.M. thanks the University of Sydney Sesqui Postdoctoral Fellowship scheme for its support.

Supporting Information Available: Projected density of states. This material is available free of charge via the Internet at http://pubs.acs.org.

References and Notes

(1) Christmann, K. Hydrogen Adsorption at Metal Surfaces. In *Electrocatalysis. Frontiers of Electrochemistry*; Lipkowsky, J., Ross, P. N., Eds.; Wiley-VCH: New York, 1998; p 1.
(2) Christmann, K. *Surf. Sci. Rep.* **1988**, *9*, 163.
(3) Halstead, D.; Holloway, S. *J. Chem. Phys.* **1990**, *93*, 2859.
(4) Gross, A. Ab Initio Molecular Dynamics Simulations of Reactions at Surfaces. In *Computer Simulation of Materials at Atomic Level*; Deak, P., Frauenheim, T., Pederson, M. R., Eds.; Wiley-VCH: Berlin, 2000; p 389.
(5) Yu, C. F.; Whaley, K. B.; Hogg, C. S.; Sibener, S. J. *Phys. Rev. Lett.* **1983**, *51*, 2210.
(6) Horne, J. M.; Yerkes, S. C.; Miller, D. R. *Surf. Sci.* **1980**, *93*, 47.
(7) Asada, H. *Surf. Sci.* **1979**, *81*, 386.
(8) Canepa, M.; Cantini, P.; Cavanna, E.; Mattera, L.; Tarditi, V.; Terreni, S. *Surf. Sci.* **1991**, *251−252*, 1142.
(9) Healey, F.; Carter, R. N.; Worthy, G.; Hodgson, A. *Chem. Phys. Lett.* **1995**, *243*, 133.
(10) Cottrell, C.; Carter, R. N.; Nesbitt, A.; Samson, P.; Hodgson, A. *J. Chem. Phys.* **1997**, *106*, 4714.
(11) Eichler, A.; Hafner, J.; Gross, A.; Scheffler, M. *Phys. Rev. B: Condens. Matter* **1999**, *59*, 13297.
(12) Zhou, X. L.; White, J. M.; Koel, B. E. *Surf. Sci.* **1989**, *218*, 201.
(13) Parker, D. H.; Jones, M. E.; Koel, B. E. *Surf. Sci.* **1990**, *233*, 65.
(14) Lee, G.; Sprunger, P. T.; Okada, M.; Poker, D. B.; Zehner, D. M.; Plummer, E. W. *J. Vac. Sci. Technol., A* **1994**, *12*, 2119.
(15) Healey, F.; Carter, R. N.; Hodgson, A. *Surf. Sci.* **1995**, *328*, 67.
(16) Koper, M. T. M.; van Santen, R. A. *J. Electroanal. Chem.* **1999**, *472*, 126.
(17) Mijoule, C.; Russier, V. *Surf. Sci.* **1991**, *254*, 329.
(18) Chase, M. W. *JANAF Thermochemical Tables, American Chemical Society and the Americal Institute of Physics for the National Bureau of Standards*, 3rd ed.; 1986.
(19) Greeley, J.; Mavrikakis, M. *J. Phys. Chem. B* **2005**, *109*, 3460.
(20) Xu, Y.; Greeley, J.; Mavrikakis, M. *J. Am. Chem. Soc.* **2005**, *127*, 12823.

(21) Eichler, A.; Hafner, J.; Kresse, G. *Surf. Rev. Lett.* **1997**, *4*, 1347.
(22) Eichler, A.; Kresse, G.; Hafner, J. *Surf. Sci.* **1998**, *397*, 116.
(23) Qin, C.; Whitten, J. L. *J. Phys. Chem. B* **2005**, *109*, 8852.
(24) Lee, G.; Plummer, E. W. *Phys. Rev. B: Condens. Matter* **1995**, *51*, 7250.
(25) Hammer, B.; Hansen, L. B.; Nørskov, J. K. *Phys. Rev. B* **1999**, *59*, 7413.
(26) Bahn, S. R.; Jacobsen, K. W. *Comput. Sci. Eng.* **2002**, *4*, 56.
(27) Vanderbilt, D. *Phys. Rev. B* **1990**, *41*, 7892.
(28) Perdew, J. P.; Chevary, J. A.; Vosko, S. H.; Jackson, K. A.; Pederson, M. R.; Singh, D. J. *Phys. Rev. B* **1992**, *46*, 6671.
(29) Hohenberg, P. C.; Kohn, W. *Phys. Rev* **1964**, *136*, B864.
(30) Monkhorst, H. J.; Pack, J. D. *Phys. Rev. B* **1976**, *13*, 5188.
(31) Neugebauer, J.; Scheffler, M. *Phys. Rev. B* **1992**, *46*, 16067.
(32) Mills, G.; Jonsson, H.; Schenter, G. K. *Surf. Sci.* **1995**, *324*, 305.
(33) Jonsson, H.; Mills, G.; Jacobsen, K. W. *Classical and Quantum Dynamics in Condensed Phase Simulations*; World Scientific: Singapore, 1998.
(34) Henkelman, G.; Uberuaga, B. P.; Jonsson, H. *J. Chem. Phys.* **2000**, *113*, 9901.
(35) Lee, G.; Plummer, E. W. *Surf. Sci.* **2002**, *498*, 229.
(36) Lee, G.; Plummer, E. W. *Phys. Rev. B: Condens. Matter* **2000**, *62*, 1651.
(37) Hammer, B.; Norskov, J. K. *Nature (London)* **1995**, *376*, 238.
(38) Zhukov, V.; Rendulic, K. D.; Winkler, A. *Vacuum* **1996**, *47*, 5.
(39) Chelvayohan, M.; Mee, C. H. B. *J. Phys. C: Solid State Phys* **1982**, *15*, 2305.
(40) Millar, G. J.; Nelson, M. L.; Uwins, P. J. R. *J. Chem. Soc., Faraday Trans.* **1998**, *94*, 2015.
(41) Millar, G. J.; Nelson, M. L.; Uwins, P. J. R. *J. Catal.* **1997**, *169*, 143.
(42) Waterhouse, G. I. N.; Bowmaker, G. A.; Metson, J. B. *Appl. Catal., A* **2004**, *265*, 85.
(43) Scheffer, M.; Stampfl, C. Theory of Adsorption on Metal Substrates. In *Handbook of Surface Science*; Horn, K., Scheffer, M., Eds.; Elsevier: Amsterdan, 2000; Vol. 2, p 285.
(44) Winkler, A. *Vacuum* **1995**, *46*, 1241.
(45) Van Slooten, U.; Kirchner, E. J. J.; Kleyn, A. W. *Surf. Sci.* **1993**, *283*, 27.
(46) Jacobi, K. *J. Electron Spectrosc. Relat. Phenom.* **1998**, *96*, 23.
(47) Eichler, A.; Hafner, J.; Kresse, G. *Surf. Rev. Lett.* **1997**, *4*, 1297.
(48) Wipf, H. *Top. Appl. Phys.* **1997**, *73*, 51.
(49) Gross, A.; Hammer, B.; Scheffler, M.; Brenig, W. *Phys. Rev. Lett.* **1994**, *73*, 3121.
(50) Eckart, C. *Phys. Rev.* **1930**, *35*, 1303.
(51) Klier, K.; Hess, J. S.; Herman, R. G. *J. Chem. Phys.* **1997**, *107*, 4033.
(52) Wigner, E. *Z. Phys. Chem.* **1932**, *B19*, 203.
(53) Truhlar, D. G.; Kuppermann, A. *J. Am. Chem. Soc.* **1970**, *93*, 1840.
(54) Le Roy, R. J.; Quickert, K. A.; Le Roy, D. J. *Trans. Faraday Soc.* **1970**, *66*, 2997.
(55) Klier, K. *Top. Catal.* **2002**, *18*, 141.
(56) Verhoef, R. W.; Kelly, D.; Mullins, C. B.; Weinberg, W. H. *Surf. Sci.* **1994**, *311*, 196.
(57) Stern, M. J.; Weston, R. E., Jr. *J. Chem. Phys.* **1974**, *60*, 2803.
(58) http://www.reactiondesign.com/.
(59) Vincent, J. K.; Olsen, R. A.; Kroes, G.-J.; Luppi, M.; Baerends, E.-J. *J. Chem. Phys.* **2005**, *122*, 044701.
(60) Murphy, M. J.; Hodgson, A. *Phys. Rev. Lett.* **1997**, *78*, 4458.
(61) Schober, H. R.; Stoneham, A. M. *Phys. Rev. Lett.* **1988**, *60*, 2307.
(62) Sundell, P. G.; Wahnstroem, G. *Surf. Sci.* **2005**, *593*, 102.
(63) Luntz, A. C.; Harris, J. *Surf. Sci.* **1991**, *258*, 397.
(64) DeWitt, K. M.; Valadez, L.; Abbott, H. L.; Kolasinski, K. W.; Harrison, I. *J. Phys. Chem. B* **2006**, *110*, 6705.